

Discovering benzamide derivatives as glycogen phosphorylase inhibitors and their binding site at the enzyme

Ling Chen,^a Honglin Li,^{a,b,*} Jun Liu,^c Luyong Zhang,^c Hong Liu^{a,*} and Hualiang Jiang^{a,d}

^a*Drug Discovery and Design Center, State Key Laboratory of Drug Research, Shanghai Institute of Materia Medica, Shanghai Institutes for Biological Sciences, Chinese Academy of Sciences, 555 Zu Chong Zhi Road, Shanghai 201203, PR China*

^b*Department of Engineering Mechanics, State Key Laboratory of Structural Analyses for Industrial Equipment, Dalian University of Technology, Dalian 116023, PR China*

^c*Jiangsu Center for Drug Screening, China Pharmaceutical University, Nanjing 210038, PR China*

^d*School of Pharmacy, East China University of Science and Technology, Shanghai 200237, PR China*

Received 29 June 2007; revised 31 July 2007; accepted 1 August 2007

Available online 10 August 2007

Abstract—A series of novel benzamide derivatives was designed, synthesized, and their inhibitory activities against glycogen phosphorylase (GP) in the direction of glycogen synthesis by the release of phosphate from glucose-1-phosphate were evaluated. The structure-activity relationships (SAR) of these compounds are also presented. Within this series of compounds, **4m** is the most potent GP_a inhibitor (IC₅₀ = 2.68 μM), which is nearly 100 times more potent than the initial compound **1**. Analysis of mapping between pharmacophores of different binding sites and each compound demonstrated that these benzamide derivatives bind at the dimer interface of the rabbit muscle enzyme, and possible docking modes of compound **4m** were explored by molecular docking simulation. © 2007 Elsevier Ltd. All rights reserved.

1. Introduction

Type 2 diabetes is a complex and prevalent disease characterized by hyperglycemia. It has become the fourth leading cause of death and affects ~150 million people worldwide, and its prevalence is expected to double by the year 2025.¹ However, current therapies do not achieve adequate control of glycemia in type 2 diabetes,² and abundant use of combination therapy to attempt to reach optimal glycemia control indicates that it is difficult to control the disease by attacking only one pathway.³ Therefore, there is a growing demand for novel drugs with safer and more effective anti-diabetic therapies.

In type 2 diabetes state, elevated hepatic glucose production (HGP) by glycogenolysis and gluconeogenesis is a contributing factor to hyperglycemia.⁴ In muscle and liver, glycogen concentrations are regulated by the coor-

dated activities of glycogen synthase and glycogen phosphorylase (GP).⁵ GP is responsible for the release of glucose-1-phosphate from glycogen, which is the first and the rate-limiting step in the glycogenolysis reaction.⁶ GP exists in two interconvertible forms, GP_a (the phosphorylated form, high activity, high substrate affinity, predominantly R state) and GP_b (the nonphosphorylated form, low activity, low substrate affinity, predominantly T state).⁷ Therefore, the inhibitors of GP_a (more active form) will limit glycogen degradation and reduce HGP, which provide new potential therapeutic agents for the treatment of type 2 diabetes.

During the last decade, GP inhibitors have attracted considerable attention. Several classes of small molecule inhibitors of GP have been reported.⁸ There are at least six known binding sites in the GP enzyme: glucose analogues⁹ binding to the catalytic site, flavopiridol¹⁰ and olefin analogues⁴ binding to the inhibitor site (also referred to as the purine nucleoside site), diacid analogues¹¹ and 5-chloroindole glycine amide inhibitors¹² binding to the allosteric AMP site, thienopyrrole inhibitors¹³ and 1-substituted-3,4-dihydro-2-quinolone inhibitors¹⁴ binding at the dimer interface site (or an indole carboxamide site), the glycogen storage site and Ser14-phosphate recognition site. Among them, the former

Keywords: Glycogen phosphorylase (GP) inhibitors; Binding site; Structure-based pharmacophore; Molecular docking.

*Corresponding authors. Tel.: +86 21 50807042; fax: +86 21 50807088; e-mail addresses: hlli@mail.shnc.ac.cn; hliu@mail.shnc.ac.cn

four regulatory sites are known to be inhibitor binding sites.

Compounds with the benzamide core have been widely studied due to their capability of binding to many receptors with high affinity. By screening abundant substituted benzamide compounds of our in-house collection, 2-amino-4-fluoro-5-(1-methyl-1*H*-imidazol-2-ylthio)-*N*-phenylbenzamide (**1**, Fig. 1), *N*¹,*N*⁴-di(thiazol-2-yl)terephthalamide (**2**, Fig. 1), and 2-(4-phenylpiperazin-1-yl)-*N*-(thiazol-2-yl)acetamide (**3**, Fig. 1) were identified as GP inhibitors with IC₅₀ values of 214.6, 337.1, and 96.9 μM, respectively. In this paper, using the screening hits **1–3** as the benchmark compounds, a series of novel benzamide derivatives (**4a–n**, **5a–f** and **6a–c**, Tables 1–3) were designed, synthesized and their inhibitory activities against GP enzyme in the direction of glycogen synthesis by the release of phosphate from glucose-1-phosphate were measured. The structure–activity relationship analyses of these inhibitors were also performed in this study.

X-ray structural experimental assays are very time-consuming and labour intensive, and competitive binding studies are not suitable to identify the binding sites of these inhibitors. In order to identify the binding site of these benzamide derivatives with GP, we analyzed the mapping between each compound and pharmacophores which are based on complexes with known ligands bound at different binding sites, and demonstrated that these benzamide derivatives bind at the dimer interface of the rabbit muscle GP enzyme. The probable binding site of the inhibitors to GP was further verified by molecular docking simulation. Consequently, analysis of structure-based pharmacophore method plays an exemplary role in discovering the drug, especially selective drug, for multiple targets or binding sites.

2. Materials and methods

2.1. Chemistry

2.1.1. Design of the derivatives of GP inhibitors. Based on the structural feature of the screening hits **1–3**, 23 compounds (**4a–n**, **5a–f**, and **6a–c**) were designed and synthesized. Compounds **4a–n** were derived from compound **1** by adding different substitutions to the phenyl group. Keeping the phenyl ring of compound **2** and replacing the thiazole ring with various substituted heterocycles produced derivatives **5a–f**. Compounds **6a–c** were obtained by introducing 2-OCH₃ and 2-F substitu-

tions to phenyl ring and replacing thiazole ring of **3**-CF₃ substituted phenyl.

2.1.2. Synthetic procedures. Scheme 1 depicts the sequence of reactions that led to the preparation of compounds **4a–n** using 4,5-difluoro-2-nitrobenzoic acid as the starting material. In general, treatment of 4,5-difluoro-2-nitrobenzoic acid with oxalyl dichloride and DMF afforded 4,5-difluoro-2-nitrobenzoyl chloride **7**. Then **7** reacted with appropriate commercially available aniline to give benzamide **8a–n**. Reaction of **8a–n** with 1-methyl-1*H*-imidazole-2-thiol and triethylamine provided **9a–n**. And compounds **4a–n** were obtained by hydrogenizing **9a–n** catalyzed by iron powder and saturated aqueous NH₄Cl.

The series of symmetrical benzamide analogues **5a–f** were synthesized by isophthaloyl dichloride or terephthaloyl dichloride reacting with aniline in the presence of pyridine or triethylamine as shown in Scheme 2. The series of piperazine-containing amide analogues **6a–c** were prepared from 1-(2-R₂-phenyl) piperazine and **10a–c** which were produced by the reaction of 2-chloroacetyl chloride with amino compounds as shown in Scheme 3.

2.2. Glycogen phosphorylase enzyme assays

2.2.1. Materials. Glycogen phosphorylase a (from rabbit muscle), glycogen, glucose-1-phosphate, malachite green, and ammonium molybdate were purchased from the Sigma–Aldrich Corporation (St. Louis, MO, USA). Reagents and solvents were obtained from commercial suppliers and used without further purification. Solvents used were AR grade.

2.2.2. Enzymatic activity assay. The enzymatic inhibition of phosphorylase activity was monitored using microplate reader (Bio-Rad) based on the published methods.¹⁵ In brief, GP activity was measured in the direction of glycogen synthesis by the release of phosphate from glucose-1-phosphate. Each compound was dissolved in DMSO and diluted at different concentrations for IC₅₀ determination. The enzymes were added into the 100 μL buffer with compounds dissolved in containing 50 mM Hepes (pH 7.2), 100 mM KCl, 2.5 mM MgCl₂, 0.5 mM glucose-1-phosphate, and 1 mg/mL glycogen in 96-well microplates (Costar). After the addition of 150 μL of 1 M HCl containing 10 mg/mL ammonium molybdate and 0.38 mg/mL malachite green, reactions were run at 22 °C for 25 min. And then the phosphate absorbance was measured at 655 nm. The IC₅₀ val-

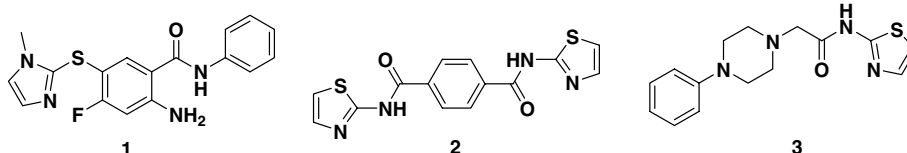
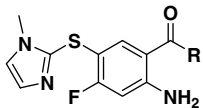
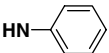
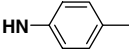
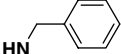
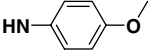
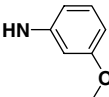
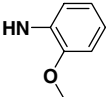
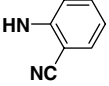
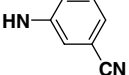


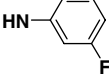
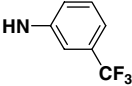
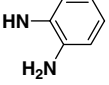
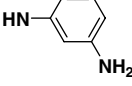
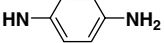


Figure 1. The structures of compounds **1–3**, which appeared as potential leads in a focused database screening.

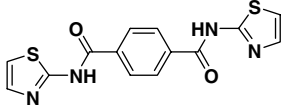
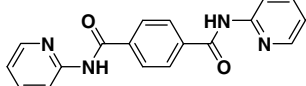
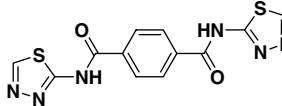
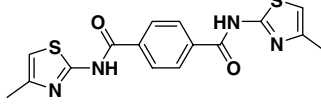
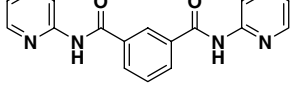
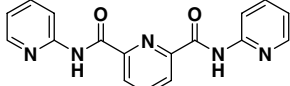
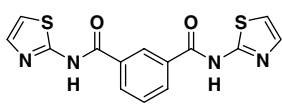
Table 1. Chemical structure of compounds **1**, **4a–n** and their activities

		
Compound	R	RMGPa IC ₅₀ (μM) ^a
1		214.6
4a		70.1
4b		152.8
4c		107.4
4d		165.6
4e		41.8
4f		75.9
4g		9.87
4h		96.1
4i		ND ^b
4j		30.9
4k		8.95
4l		95.3
4m		2.68
4n		91.1

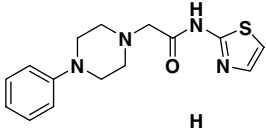
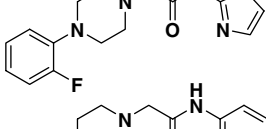
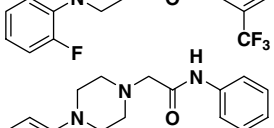
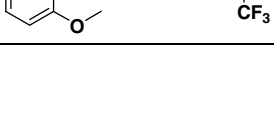
^a Caffeine was used as control.^b ND, not determined.

ues were estimated by fitting the inhibition data to a dose-dependent curve using a logistic derivative equation.

Table 2. Chemical structures of compounds **2**, **5a–e** and their activities

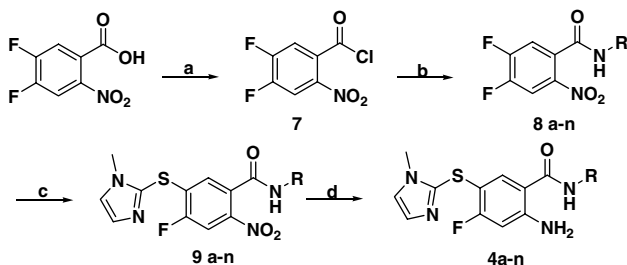
Compound	Structure	RMGPa IC ₅₀ (μM) ^a
2		337.1
5a		ND ^b
5b		269.1
5c		ND ^b
5d		57.6
5e		425
5f		ND ^b

^a Caffeine was used as control.^b ND, not determined.**Table 3.** Chemical structures of compounds **3**, **6a–c** and their activities

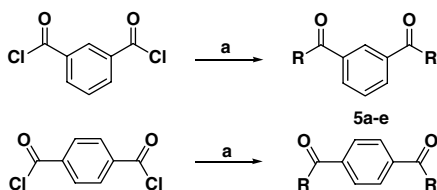
Compound	Structure	RMGPa IC ₅₀ (μM)
3		96.9
6a		35.8
6b		78.5
6c		46.1

2.3. Binding site prediction through analysis of mapping between each compound probe and pharmacophore

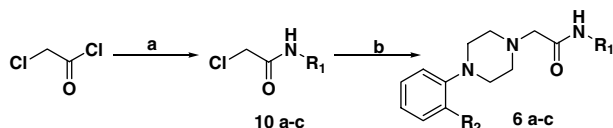
The structure-based pharmacophore models for four different binding sites were created using LigandScout¹⁶



Scheme 1. Reagents and conditions: (a) oxalyl chloride (1.2 equiv), DMF (two drops), CH_2Cl_2 , rt, 2 h; (b) R-NH_2 (1 equiv), pyridine (2 equiv), CH_2Cl_2 , rt; (c) 1-methyl-1H-imidazole-2-thiol (1 equiv), Et_3N (3 equiv), CH_3CN , reflux; (d) iron powder (10 equiv), isopropanol, reflux, 0.5 h.



Scheme 2. Reagents and conditions: (a) $\text{NH}_2\text{-R}$ (2 equiv), pyridine or triethylamine (5 equiv), CHCl_3 , rt, 12 h.



Scheme 3. Reagents and conditions: (a) $\text{R}_1\text{-NH}_2$ (1 equiv), K_2CO_3 (2 equiv), THF, 45 °C, 2 h; (b) 1-(2- R_2 -phenyl)piperazine (1 equiv), KI (catalyzer), K_2CO_3 (2 equiv), THF, 50 °C, 4 h.

against several protein–ligand complexes (Fig. S1). Four different binding sites (Fig. 2) were derived from the crystal structures of GP with known inhibitors: Caffeine and Flavopiridol at the inhibitor site (PDB entry 1C8K¹⁰ and 1GFZ¹⁷); Bzurea at the catalytic site (PDB entry 1K06¹⁸); BAY-W1807, acyl urea inhibitor, at the AMP allosteric site (PDB entry 3AMV,¹⁹ 2ATI,²⁰ 1Z6P,²¹ and 1Z6Q²¹); Thienopyrrole inhibitors, such as Bzurea and CP320626, at the dimer interface site (PDB entry 2GJ4,²² 2GM9,²² 1K06,¹⁸ 1H5U,²³ and 2IEI²⁴). Analysis of mapping between each compound and pharmacophores was implemented according to the following process: (i) each pharmacophore model, representing a class of binding interactions at different binding sites, was generated by LigandScout with the complex structure; (ii) compounds **4e**, **4j**, **4g**, **4k**, **4m**, and **6a** were used as probes to fit the pharmacophore models of different binding sites using Catalyst software²⁵; (iii) the pharmacophores were found with which the compounds match best.

The structures of compounds were built using Catalyst 2D–3D sketcher, and conformations of each compound were generated with maximum 255 conformers using best quality generation type, and 20.0 kcal/mol was the

allowed energy range for the conformers above the global energy minimum in the conformational space.

2.4. Molecular docking simulation

After identifying the most likely binding site for these inhibitors through the above-mentioned analysis, more extensive docking simulation was performed to further verify the binding model between inhibitors and GP. Autodock3.05 software²⁶ was used for the docking simulations. The high resolution crystal structure 2IEI¹⁴ (RMGPa complex with FXR at the dimer interface site) was used as the target for docking simulation. Ligand and water molecules in the crystal structure were removed, polar hydrogens were added, and ‘KOLLUA’ charges²⁷ were assigned to the protein. The conformations of compounds best fit to pharmacophore mentioned above were used as the initial structures for docking, and Gasteiger–Marsilli charges were assigned to the compounds. Since the dimer interface site is formed by residues from both monomers, to ensure the searching space enclosing the binding site, the numbers of grid points were set as 100 in x , y , and z directions around the central point of the dimer. The Lamarckian genetic algorithm (LGA)²⁶ was adopted in the molecular docking simulation, and the number of individuals for the population was set as 150, correspondingly, the maximum number of energy evaluations and the maximum numbers of generations were set as 4,500,000 and 81,000, respectively. Twenty independent runs with different seeds were performed on a SGI origin 3800 supercomputer. The ligand was fully optimized inside the binding site during the docking simulations, and the best docking modes were determined by choosing those poses with the lowest energy for each ligand.

3. Results and discussion

3.1. Biological activities on rat muscle glycogen phosphorylase a (RMGPa)

The enzymatic inhibition activities of compounds **1–3**, **4a–n**, **5a–f**, and **6a–c** against GP_a determined by the methods described in Section 2.2 are listed in Table 1. The hit, compound **1**, exhibits a medium inhibitory activity toward GP_a with an IC_{50} value of 214.6 μM . After inserting a methylene group between the amide nitrogen and the phenyl ring, compound **4b** maintains the similar potency. Introducing methoxyl group (**4c**, **4d**, **4e**), cyano group (**4f**, **4g**, **4h**), fluorine (**4j**), trifluoromethyl group (**4k**), and amino group (**4l**, **4m**, **4n**), to the phenyl group apparently increased the inhibitor potency. The 3- NH_2 derivative (**4m**) with an IC_{50} value of 2.68 μM showed the most potent inhibitory activity among the compounds. Compound **4g** (3-CN), **4j** (3-F), and **4k** (3- CF_3) also exhibited good results, with the IC_{50} values of 9.87, 30.9, and 8.95 μM , respectively. However, moving the 3-fluorine substitute to 2,6-position (**4i**) led to a complete loss of activity.

Compound **2** is less active toward GP_a with an IC_{50} value of 337 μM . The inhibitor potencies were slightly

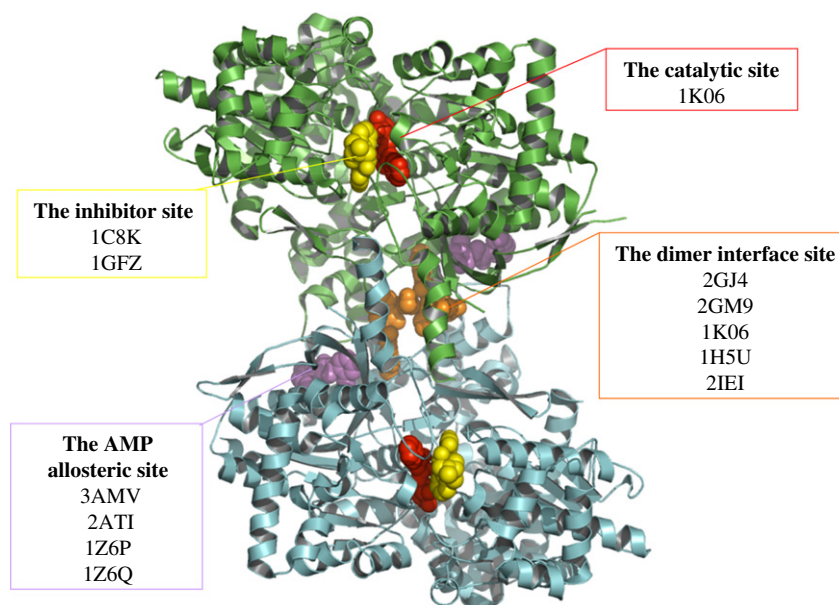


Figure 2. Schematic diagram of the GP dimeric molecule viewed down the molecular dyad. One subunit is colored in green and the other in cyan. Four different categories of inhibitor sites are highlighted through CPK models of the respective ligands. The catalytic site is colored in red, corresponding complex is **1K06**. The inhibitor site is colored in yellow, corresponding complexes are **1C8K** and **1GFZ**. The AMP allosteric site is colored in magenta, corresponding complexes are **3AMV**, **2ATI**, **1Z6P**, and **1Z6Q**. The dimer interface site is colored in orange, corresponding complexes are **2GJ4**, **2GM9**, **1K06**, **1H5U**, and **2IEI**. The dimer interface site, located inside the central cavity and formed by the two subunits, is approximately 15 Å from the allosteric AMP site, 33 Å from the catalytic site, and 37 Å from the inhibitor site. The structure-based pharmacophore models for four different binding sites were created against these GP–ligand complexes. Compounds **4e**, **4g**, **4k**, **4j**, **4m**, and **6a** were used as probes to fit the pharmacophore models of different binding sites (Table 4).

increased by replacing the thiazole ring with 1,3,4-thiadiazole group (**5b**) as shown in Table 2. When replacing the terephthaloyl dichloride with isophthaloyl dichloride, the activity of compound **5d** ($IC_{50} = 57.6 \mu M$) was apparently increased. However, when the phenyl of **5d** was changed to pyridine ring (**5e**), the potency of compound was lost. The activities of these symmetrical benzamide analogues were not as good as the activities of compounds **4a–n**, due to the loss of the amino group of the middle phenyl and the rigidity of two carbonyl groups.

By adding the 2-F group to the phenyl ring of compound **3** ($IC_{50} = 96.9 \mu M$), the inhibition potency (**6a**) was increased. While introducing the 3-(trifluoromethyl)benzenamine group to compound **3** gave a more potent inhibitor (**6b**, **6c**).

3.2. Prediction of potential binding site

Competitive binding studies are not suitable to identify the binding sites of benzamide derivatives,²⁸ and the binding sites of GP are relatively dispersed in the GP dimer.²³ For example, the dimer interface site, which located inside the central cavity and formed by the two subunits, is approximately 15 Å from the allosteric AMP site, 33 Å from the catalytic site, and 37 Å from the inhibitor site (Fig. 2). Accordingly, it is unsuitable and inaccurate to implement molecular optimization to find the binding sites of our inhibitors by using molecular docking method in such an immense searching space.

To identify the probable binding site fast and accurately, compounds **4e**, **4g**, **4k**, **4j**, **4m**, and **6a** were used to map to the pharmacophores derived from the crystal structures of inhibitor-GP complexes (see Section 2). The glycogen storage site and Ser14-phosphate recognition site were not considered because they are not inhibitor binding sites as mentioned above. From Table 4, we can see that no mapping was possible in comparing operations between these compounds and the pharmacophore of complex 1C8K in the inhibitor site. Although these compounds were able to fit to the pharmacophore of complex 1GFZ more or less (Fig. 3a), it requires these compounds to conquer more conformation energy (12.5251, 13.6558, 5.44196, 11.2092, 3.91966, and 13.2133 kcal/mol, respectively). For the catalytic site, these compounds also could not be fitted to the pharmacophore of complex 1K06. The catalytic site was known as the binding site of glucose analogues. However, if Bzurea bound at the dimer interface site of complex 1K06, these compounds can fit the pharmacophore very well (see footnote of Table 4). Because of considering the interaction between the bound ligand and protein including key water molecules, all these compounds were able to fit those pharmacophores of complexes with ligands bound at the dimer interface site. The mapping of compound **4m** and pharmacophore of complex 2IEI is shown in Figure 3b. Most of the compounds were not able to fit to those pharmacophores of complexes with ligands bound at the AMP allosteric site, except for 2ATI case. These compounds have some 3D similarities with the ligand in the 2ATI complex (Fig. 4a), but the interactions with protein are incorrect

Table 4. The fit values of compounds compared with pharmacophore based on complex structures for four different categories binding sites

	4e	4g	4k	4j	4m	6a
The inhibitor site						
1C8K	N/M [*]	N/M	N/M	N/M	N/M	N/M
1GFZ	2.13258	2.2104	2.12344	2.17843	2.19227	1.75998
The catalytic site						
1K06 ^a	N/M	N/M	N/M	N/M	N/M	N/M
The dimer interface site						
2GJ4	1.8799	1.92384	2.04043	1.98176	2.57069	1.64323
2GM9	2.4409	1.97927	2.39471	2.17587	2.01597	2.35093
1K06 ^b	2.141987	1.54151	2.6116	1.56013	1.93331	1.653628
1H5U	2.49269	2.17955	3.21127	2.42967	2.75289	2.54755
2IEI	2.81157	2.90281	3.34978	2.83311	2.80239	2.88392
The AMP allosteric site						
3AMV	N/M	N/M	N/M	N/M	N/M	N/M
2ATI	2.5911	2.62288	3.01083	2.3964	2.94731	N/M
1Z6P	N/M	N/M	N/M	N/M	N/M	N/M
1Z6Q	N/M	N/M	N/M	N/M	N/M	N/M

Compounds **4e**, **4g**, **4k**, **4j**, **4m**, and **6a** were used as probe to fit the pharmacophore models of different binding sites.

^a Bzurea bound at the catalytic site.

^b Bzurea bound at the dimer interface site.

* N/M: no mapping was possible in compare operation.

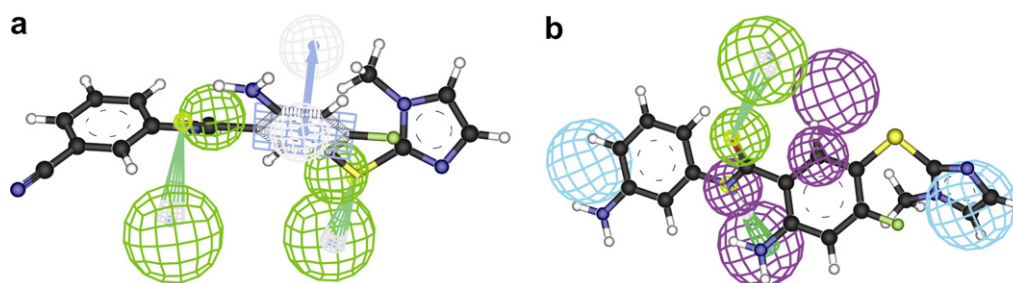


Figure 3. Mapping of compounds **4g** and **4m** onto the structure-based pharmacophore model. Pharmacophoric features are hydrogen-bond acceptor (green), hydrogen-bond donor (magenta), hydrophobic group (cyan), and aromatic ring (orange). (a) Mapping of compound **4g** onto the pharmacophore for the inhibitor site based on the complex structure (1GPZ), with fit value of 2.2104 and conformation energy of 13.6558 kcal/mol; (b) Mapping of compound **4m** onto the pharmacophore for the dimer interface site based on the complex structure (2IEI), with fit value of 2.80239 and conformation energy of 4.39393 kcal/mol.

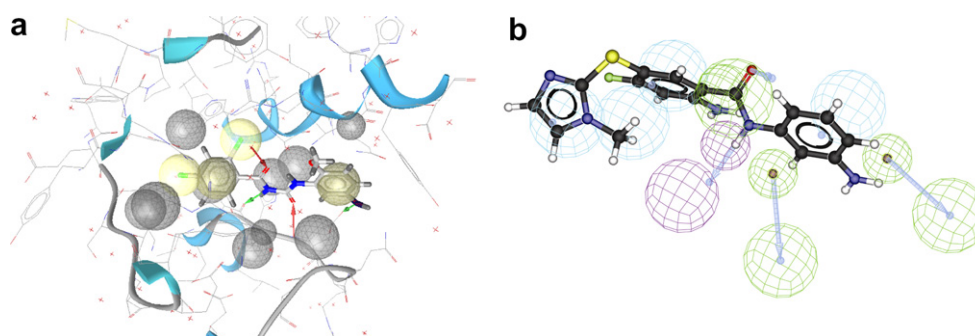


Figure 4. The pharmacophore for the AMP allosteric site. (a) The pharmacophore based on the complex structure (2ATI) with acyl urea inhibitor. Pharmacophore features are hydrogen-bond acceptor (red arrow), hydrogen-bond donor (green arrow), hydrophobic groups (yellow sphere), and excluded volume (gray sphere). (b) Mapping of compound **4m** onto the pharmacophore using Catalyst 4.10. Pharmacophoric features are hydrogen-bonds acceptor (green), hydrogen-bond donor (magenta), and hydrophobic group (cyan).

after comparing with and fitting to the pharmacophore in catalyst (Fig. 4b), due to lack of three important hydrogen-bond acceptor features. The pharmacophore of the AMP allosteric site used here generated by

LigandScout was very similar to that in the original paper,²⁰ which indicates that the complex structure-based pharmacophore is more reliable. Through analysis of mapping to each binding site, it appeared that

our compounds likely bind at the dimer interface site. This prediction will be subsequently validated by our X-ray crystal structure experiment in our future work.

3.3. Binding model predicted by molecular docking simulation

After identifying the dimer interface site as the most likely binding site for these compounds, the crystal structure of RMGP complexed with ligand bound at the dimer interface site (PDB entry 2IEI) was selected for use in the molecular docking simulation. The first ranked docking conformation of compound **4m** at the dimer interface, with the best interaction energy (−8.42 kcal/mol), was determined as a preferred docking mode, as shown in Figure 5. One can clearly see (Figs. 5

and 6b) that this inhibitor binds at the dimer interface, which forms the binding site for the inhibitor with many hydrophobic residues including Trp67 (A), Leu63(A), Trp189 (A), Lys191 (A), Ala192 (A), Pro229 (A), and Leu39 (B). 1-Methylimidazole and the 3-aminophenyl groups are bordered by this hydrophobic site. The nitrogen of 3-aminophenyl is close to Arg60 (A) to which it may form a hydrogen bond, and the nitrogen of the amide carbonyl group forms a hydrogen bond with the oxygen of Pro188 (A). It should be noted that the amino group of the middle phenyl can form three hydrogen bonds with Asn187 (A), Pro188 (A), and Glu190 (A), respectively, which may provide stable interaction. The interactions were in accord with those presented in the pharmacophore based on complex structure of GPa (Fig. 3b).

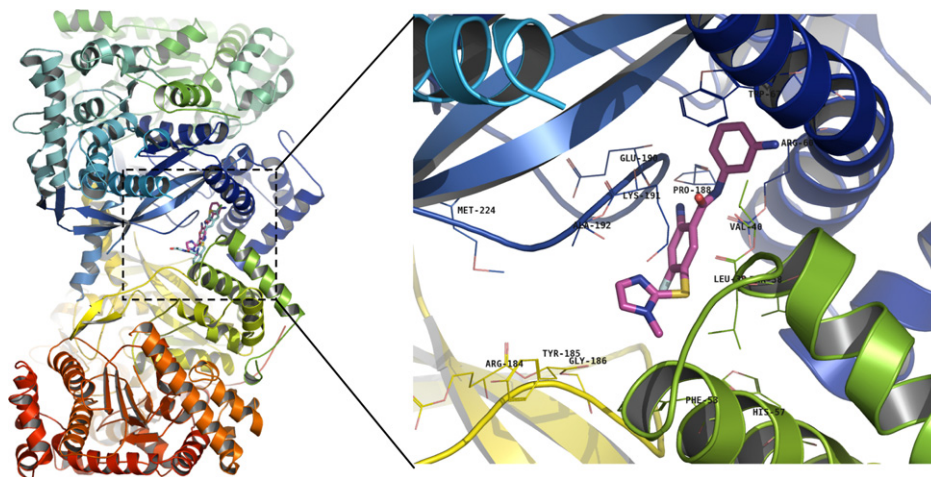


Figure 5. Stereoview of the binding mode of compound **4m** at the dimer interface site of RMGP (left) and enlarged view of binding site (right) with residues around the docked pose within 4.0 Å. The RMGP structure is shown in cartoon, and residues in the binding site are shown in line. The coloring for **4m** is as follows: carbon atoms, magenta; oxygen atoms, red; nitrogen atoms, blue; sulfur atoms, yellow; fluorine, cyan; respectively. Hydrogen atoms have been omitted for clarity. All structure figures were prepared using PyMol (<http://pymol.sourceforge.net/>).

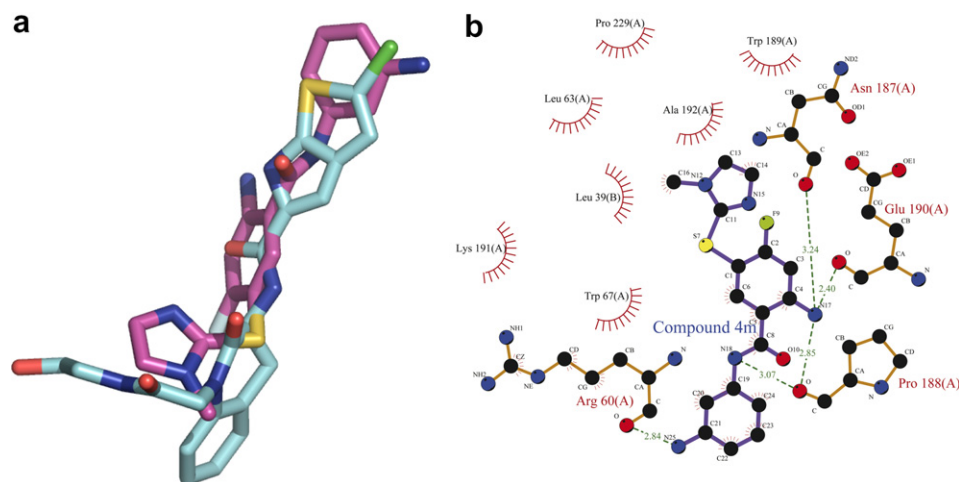


Figure 6. (a) Comparison of docked compound **4m** with the ligand bound in crystal structure (2IEI). Compound **4m** (carbons in magenta) and ligand of FRX (carbon in cyan) are shown in stick with the non-carbon atoms in standard colors. Hydrogen atoms have been omitted for clarity. (b) Two-dimensional representation for the interacting mode of compound **4m** with RMGP. A distance between donor and acceptor less than 3.4 Å is considered as a hydrogen-bond, and a 4.1-Å distance between two hydrophobic atoms is considered hydrophobic interaction. The hydrogen bonds and hydrophobic interactions were calculated by HBPLUS and LIGPLOT,³¹ respectively. Dashed lines represent hydrogen bonds, and spiked residues form hydrophobic contacts with the ligands.

The predicted docking conformation occupies the same location of its bound ligand (FRX) at the dimer interface site in crystal structure (Fig. 6a and b). Same as the interaction of FRX, two ends of compound **4m** are overlaid with 1-methylimidazole and the 3-aminophenyl group interacting with those hydrophobic residues, moreover, 3-amino group of the benzamide and the nitrogen of the amide carbonyl group maintain all major interactions of hydrogen bonds. It also displayed the same orientation and presented ideal superposition between the docked conformation of **4m** and FRX in crystal structure (Fig. 6a).

The nitrogen of the amide carbonyl group of this series of compounds forms a hydrogen bond with the oxygen of Pro188 (A), and the amino group of the middle phenyl can form three hydrogen bonds with Asn187 (A), Pro188 (A), and Glu190 (A). The activities of 3-position substituted compounds are much better than those of compounds which were substituted by the same group in 2- and 4-position, except the methoxyl group. This can be illustrated by the much more steric space for hydrophobic effect formed by 3-position substituted phenyl with enzyme and the hydrogen bond formed by 3-position electronegative group with Arg60 (A) (Figs. 5 and 6b), which fit pharmacophores well and enhance activity further. The activities of symmetrical benzamide compounds **5a–f** were not as good as the activities of compounds **4a–n**, because of the rigidity of two amide groups and unfitness into the hydrogen bond interactions and pharmacophores discussed above. The structures of compounds **6a–c** with 2-(piperazin-1-yl)acetamide in middle are more flexible compared to **5a–f**, so the inhibitory activities are much better than those of compounds **5a–f**.

4. Conclusions

In this paper, we have identified a series of novel benzamide inhibitors of glycogen phosphorylase and described their SAR, enzyme activities, and synthetic routes. Within this series of compounds, **4m** was the most potent GP α inhibitor ($IC_{50} = 2.68 \mu M$). Structure-based pharmacophore strategy was put forward to predict the potential binding site for our compounds, and analysis of mapping between each compound and pharmacophore based on complexes with ligand bound at different binding sites demonstrated that these compounds' binding sites were at the dimer interface of the RMGP enzyme. By using the crystal structure of RMGP (PDB entry 2IEI), possible docking modes of compound **4m** were further explored by Autodock calculation.

Compared to 3D similarity,^{28,29} complex structure-based pharmacophore adequately considers the interaction between the ligand and protein including some key water molecules, which is more reliable due to considering the position of molecular features in 3D space. In this paper, analysis of structure-based pharmacophore plays an exemplary role in discovering potential binding sites for inhibitors, especially for targets with multiple binding sites. Moreover, complex structure based pharmacophore

can provide guidance for the design of novel inhibitors of GP, and also can be applied in large-scale database screening. By far, more than 1000 complex structure-based pharmacophores against Potential Drug Target Database (PDTD, unpublished) have been constructed, and a new program to predict the binding site or target based on this strategy is also underway. We believe it should be possible to enable reliable prediction of binding target through combining with reverse docking method.³⁰

5. Experimental

Melting points were measured in capillary tube on a SGW X-4 melting point apparatus without correction. The type of analytical thin-layer chromatography (TLC) was HSGF 254 (0.15–0.2 mm thickness, Yantai Huiyou Company, China). Nuclear magnetic resonance (NMR) spectra were recorded on a Bruker AMX-300 NMR (TMS as IS). Chemical shifts were reported in parts per million (ppm, δ) downfield from tetramethylsilane. Proton coupling patterns were described as singlet (s), doublet (d), triplet (t), quartet (q), multiplet (m), and broad (br). Low- and high-resolution mass spectra (LRMS and HRMS) were given with electric (EI) produced by Finnigan MAT-95 mass spectrometer.

5.1. 2-Amino-4-fluoro-5-(1-methyl-1*H*-imidazol-2-ylthio)-*N*-phenylbenzamide (**1**)

4,5-Difluoro-2-nitrobenzoic acid (200 mg, 0.98 mmol) reacted with oxalyl dichloride (0.2 mL) and DMF (two drops) at room temperature for 2 h. After concentration of the reaction mixture, the residue was dissolved in CH_2Cl_2 and then added dropwise into the mixture of aniline (91 mg, 0.98 mmol) and pyridine (1.96 mmol) in CH_2Cl_2 . The mixture was stirred vigorously for 12 h at room temperature and washed with 0.1 M aqueous hydrochloric acid solution (2×50 mL), a saturated aqueous sodium bicarbonate solution (2×50 mL) and a saturated aqueous sodium chloride solution (2×50 mL) sequentially, and then dried over sodium sulfate, filtered, and concentrated in vacuum. A mixture of the obtained benzamide (190 mg, 0.68 mmol), 1-methyl-1*H*-imidazole-2-thiol (78 mg, 0.68 mmol), and triethylamine (2.05 mmol) in acetonitrile was heated to reflux with stirring overnight. Upon cooling, the yellow precipitate was filtered and washed with water (5 mL). Then deoxidizing the precipitate by iron power (2 g) and saturated aqueous NH_4Cl (2 mL) in isopropanol gave compound **1** as a white solid (157 mg, 45% total yield). Mp 108–112 °C; 1H NMR (300 Hz, CD_3OD-d_4) δ : 3.80 (3H, s), 6.49 (1H, d, $J = 11.5$ Hz), 7.00 (1H, s), 7.12–7.16 (2H, m), 7.34 (2H, t, $J = 15.7$ Hz), 7.63 (2H, d, $J = 9.6$ Hz), 7.93 (1H, d, $J = 7.9$ Hz). HRMS (EI) m/z calcd for $C_{17}H_{15}FN_4OS$ (M^+) 342.0951, found 342.0948.

5.2. 2-Amino-4-fluoro-5-(1-methyl-1*H*-imidazol-2-ylthio)-*N*-*p*-tolylbenzamide (**4a**)

In the same manner as described in the preparation of **1**, **4a** was prepared from 4-methylaniline. Total yield: 50%; mp 75–80 °C; 1H NMR (300 Hz, CD_3OD-d_4) δ : 3.79

(3H, s), 3.91 (3H, s), 6.51 (1H, d, $J = 11.5$ Hz), 6.95 (1H, t, $J = 16.6$ Hz), 7.01 (1H, d, $J = 1.4$ Hz), 7.05 (1H, d, $J = 9.3$ Hz), 7.16 (1H, t, $J = 1.73$ Hz), 7.20 (1H, d, $J = 0.5$ Hz), 7.80 (1H, d, $J = 7.8$ Hz), 7.85 (1H, dd, $J = 0.9$ Hz, 9.9 Hz). HRMS (EI) m/z calcd for $C_{18}H_{17}FN_4OS$ (M^+) 356.1107, found 356.1113.

5.3. 2-Amino-*N*-benzyl-4-fluoro-5-(1-methyl-1*H*-imidazol-2-ylthio)benzamide (4b)

In the same manner as described in the preparation of **1**, **4b** was prepared from benzylamine. Total yield: 30%; mp 163–165 °C; 1H NMR (300 Hz, CD_3OD-d_4) δ : 3.74 (3H, s), 4.50 (2H, s), 6.45 (1H, d, $J = 11.4$ Hz), 6.95 (1H, s), 7.12 (1H, s), 7.20–7.32 (5H, m), 7.79 (1H, d, $J = 7.8$ Hz). HRMS (EI) m/z calcd for $C_{18}H_{17}FN_4OS$ (M^+) 356.1107, found 356.1113.

5.4. 2-Amino-4-fluoro-*N*-(4-methoxyphenyl)-5-(1-methyl-1*H*-imidazol-2-ylthio)benzamide (4c)

In the same manner as described in the preparation of **1**, **4c** was prepared from 4-methoxyaniline. Total yield: 22%; mp 95–100 °C; 1H NMR (300 Hz, CD_3OD-d_4) δ : 3.80 (6H, d, $J = 2.1$ Hz), 6.49 (1H, d, $J = 11.7$ Hz), 6.92 (2H, d, $J = 9.3$ Hz), 6.99 (1H, s), 7.17 (1H, s), 7.51 (2H, d, $J = 9.0$ Hz), 7.91 (1H, d, $J = 8.1$ Hz). HRMS (EI) m/z calcd for $C_{18}H_{17}FN_4O_2S$ (M^+) 372.1056, found 372.1056.

5.5. 2-Amino-4-fluoro-*N*-(3-methoxyphenyl)-5-(1-methyl-1*H*-imidazol-2-ylthio)benzamide (4d)

In the same manner as described in the preparation of **1**, **4d** was prepared from 3-methoxyaniline. Total yield: 32%; mp 72–73 °C; 1H NMR (300 Hz, $DMSO-d_6$) δ : 3.72 (3H, s), 3.78 (3H, s), 6.63 (1H, d, $J = 11.7$ Hz), 6.72 (1H, d, $J = 7.2$ Hz), 6.94 (1H, s), 7.27–7.30 (3H, m), 7.40 (1H, s), 7.95 (1H, d, $J = 8.0$ Hz). HRMS (EI) m/z calcd for $C_{18}H_{17}FN_4O_2S$ (M^+) 372.1056, found 372.1059.

5.6. 2-Amino-4-fluoro-*N*-(2-methoxyphenyl)-5-(1-methyl-1*H*-imidazol-2-ylthio)benzamide (4e)

In the same manner as described in the preparation of **1**, **4e** was prepared from 2-methoxyaniline. Total yield: 51%; mp 224–225 °C; 1H NMR (300 Hz, CD_3OD-d_4) δ : 3.79 (3H, s), 3.91 (3H, s), 6.51 (1H, d, $J = 11.4$ Hz), 6.95 (1H, t, $J = 16.8$ Hz), 7.01–7.06 (2H, m), 7.13–7.21 (2H, m), 7.80 (1H, d, $J = 7.8$ Hz), 7.85 (1H, dd, $J = 0.9$ Hz, 9.6 Hz). HRMS (EI) m/z calcd for $C_{18}H_{17}FN_4O_2S$ (M^+) 372.1056, found 372.1052.

5.7. 2-Amino-*N*-(2-cyanophenyl)-4-fluoro-5-(1-methyl-1*H*-imidazol-2-ylthio)benzamide (4f)

In the same manner as described in the preparation of **1**, **4f** was prepared from 2-aminobenzonitrile. Total yield: 9%; mp 162–165 °C; 1H NMR (300 Hz, $DMSO-d_6$) δ : 3.70 (3H, s), 6.61 (1H, d, $J = 12.0$ Hz), 6.91 (1H, s), 7.27 (1H, s), 7.43 (1H, t, $J = 12.4$ Hz), 7.51 (1H, d, $J = 8.0$ Hz), 7.73 (1H, t, $J = 17.2$ Hz), 7.85 (1H, d, $J = 8.1$ Hz), 8.06 (1H, d, $J = 8.0$ Hz). HRMS (EI) m/z calcd for $C_{18}H_{14}FN_5OS$ (M^+) 367.0903, found 367.0901.

5.8. 2-Amino-*N*-(3-cyanophenyl)-4-fluoro-5-(1-methyl-1*H*-imidazol-2-ylthio)benzamide (4g)

In the same manner as described in the preparation of **1**, **4g** was prepared from 3-aminobenzonitrile. Yield: 55%; mp 172–174 °C; 1H NMR (300 Hz, $DMSO-d_6$) δ : 3.66 (3H, s), 6.57 (1H, d, $J = 11.7$ Hz), 6.88 (1H, s), 7.18 (1H, d, $J = 7.3$ Hz), 7.24 (1H, s), 7.34 (1H, t, $J = 16.3$ Hz), 7.68 (1H, d, $J = 8.3$ Hz), 7.84 (1H, s), 7.92 (1H, d, $J = 8.0$ Hz). HRMS (EI) m/z calcd for $C_{18}H_{14}FN_5OS$ (M^+) 367.0903, found 367.0977.

5.9. 2-Amino-*N*-(4-cyanophenyl)-4-fluoro-5-(1-methyl-1*H*-imidazol-2-ylthio)benzamide (4h)

In the same manner as described in the preparation of **1**, **4h** was prepared from 4-aminobenzonitrile. Total yield: 15%; mp 291–293 °C; 1H NMR (300 Hz, $DMSO-d_6$) δ : 3.71 (3H, s), 6.63 (1H, d, $J = 11.7$ Hz), 6.93 (1H, s), 7.29 (1H, s), 7.88 (5H, m). HRMS (EI) m/z calcd for $C_{18}H_{14}FN_5OS$ (M^+) 367.0903, found 367.0899.

5.10. 2-Amino-*N*-(2,6-difluorophenyl)-4-fluoro-5-(1-methyl-1*H*-imidazol-2-ylthio)benzamide (4i)

In the same manner as described in the preparation of **1**, **4i** was prepared from 2,6-difluorobenzaniline. Yield: 59%; mp 202–205 °C; 1H NMR (300 Hz, CD_3OD-d_4) δ : 3.80 (3H, s), 6.51 (1H, d, $J = 11.4$ Hz), 6.99 (1H, s), 7.07 (2H, t, $J = 12.0$ Hz), 7.17 (1H, s), 7.30–7.38 (1H, m), 8.04 (1H, d, $J = 8.1$ Hz). HRMS (EI) m/z calcd for $C_{17}H_{13}F_3N_4OS$ (M^+) 378.0762, found 378.0762.

5.11. 2-Amino-4-fluoro-*N*-(3-fluorophenyl)-5-(1-methyl-1*H*-imidazol-2-ylthio)benzamide (4j)

In the same manner as described in the preparation of **1**, **4j** was prepared from 3-fluorobenzaniline. Yield: 49%; mp 190–193 °C; 1H NMR (300 Hz, $DMSO-d_6$) δ : 3.68 (3H, s), 6.59 (1H, d, $J = 11.7$ Hz), 6.90–6.94 (2H, m), 7.25 (1H, s), 7.35–7.40 (1H, m), 7.46 (1H, d, $J = 7.5$ Hz), 7.64 (1H, d, $J = 11.7$ Hz), 7.92 (1H, d, $J = 7.5$ Hz). HRMS (EI) m/z calcd for $C_{17}H_{14}F_2N_4OS$ (M^+) 360.0856, found 360.0833.

5.12. 2-Amino-4-fluoro-5-(1-methyl-1*H*-imidazol-2-ylthio)-*N*-(3-(trifluoromethyl)phenyl)benzamide (4k)

In the same manner as described in the preparation of **1**, **4k** was prepared from 3-(trifluoromethyl)benzaniline. Yield: 34%; mp 95–100 °C; 1H NMR (300 Hz, $DMSO-d_6$) δ : 3.66 (3H, s), 6.58 (1H, d, $J = 11.7$ Hz), 6.89 (1H, s), 7.25 (1H, s), 7.42 (1H, d, $J = 7.8$ Hz), 7.56 (1H, t, $J = 16.5$ Hz), 7.90–7.97 (2H, m), 8.13 (1H, s). HRMS (EI) m/z calcd for $C_{18}H_{14}F_4N_4OS$ (M^+) 410.0824, found 410.0818.

5.13. 2-Amino-*N*-(2-aminophenyl)-4-fluoro-5-(1-methyl-1*H*-imidazol-2-ylthio)benzamide (4l)

In the same manner as described in the preparation of **1**, **4l** was prepared from 2-nitrobenzaniline. Total yield: 40%; mp 174–178 °C; 1H NMR (300 Hz, $DMSO-d_6$) δ :

3.69 (3H, s), 6.56–6.60 (2H, m), 6.76–6.79 (1H, m), 6.92–6.97 (2H, m), 7.09–7.12 (1H, m), 7.28 (1H, s), 8.00 (2H, d, $J = 8.1$ Hz). HRMS (EI) m/z calcd for $C_{17}H_{16}FN_5OS$ (M^+) 357.1060, found 357.1063.

5.14. 2-Amino-*N*-(3-aminophenyl)-4-fluoro-5-(1-methyl-1*H*-imidazol-2-ylthio)benzamide (4m)

In the same manner as described in the preparation of **1**, **4m** was prepared from 3-nitrobenzenamine. Total yield: 37%; mp 144–148 °C; 1H NMR (300 Hz, DMSO- d_6) δ : 3.63 (3H, s), 6.31 (1H, d, $J = 8.1$ Hz), 6.57 (1H, d, $J = 11.4$ Hz), 6.78 (1H, t, $J = 15.3$ Hz), 6.90 (1H, s), 6.95 (2H, t, $J = 18.9$ Hz), 7.25 (1H, s), 7.85 (1H, d, $J = 7.8$ Hz). HRMS (EI) m/z calcd for $C_{17}H_{16}FN_5OS$ (M^+) 357.1060, found 357.1052.

5.15. 2-Amino-*N*-(4-aminophenyl)-4-fluoro-5-(1-methyl-1*H*-imidazol-2-ylthio)benzamide (4n)

In the same manner as described in the preparation of **1**, **4n** was prepared from 4-nitrobenzenamine. Total yield: 45%; mp 95–98 °C; 1H NMR (300 Hz, DMSO- d_6) δ : 3.68 (3H, s), 6.52–6.57 (3H, m), 6.90 (1H, s), 7.25–7.29 (3H, m), 7.86 (1H, d, $J = 8.4$ Hz). HRMS (EI) m/z calcd for $C_{17}H_{16}FN_5OS$ (M^+) 357.1060, found 357.1068.

5.16. N^1, N^4 -Di(thiazol-2-yl)terephthalamide (2)

To a solution of thiazol-2-amine (1 g, 10 mmol) and triethylamine (25 mmol) in $CHCl_3$ (20 mL) was added terephthaloyl dichloride (1.08 g, 5 mmol) dropwise. After the mixture was stirred overnight, a saturated aqueous sodium bicarbonate solution (10 mL) was added in and reacted for another 30 min. Then compound **2** was collected by filtration, water washing, and purification as a slight yellow solid. Yield: 23%; mp >300 °C; 1H NMR (300 Hz, DMSO- d_6) δ : 7.30 (2H, d, $J = 3.3$ Hz), 7.57 (2H, d, $J = 3.9$ Hz), 8.19 (4H, s). HRMS (EI) m/z calcd for $C_{14}H_{10}N_4O_2S_2$ (M^+) 330.0245, found 330.0245.

5.17. N^1, N^4 -Di(pyridin-2-yl)terephthalamide (5a)

Compound **5a** was prepared from pyridin-2-amine (1 g, 10 mmol), pyridine (25 mmol), and terephthaloyl dichloride (1.08 g, 5 mmol) using a procedure similar to that described for the preparation of **2** as a white solid (340 mg, 21% yield). Mp 276–280 °C; 1H NMR (300 Hz, DMSO- d_6) δ : 7.19 (2H, t, $J = 12.0$ Hz), 7.86 (2H, t, $J = 17.7$ Hz), 8.11 (4H, s), 8.18 (2H, d, $J = 12.9$ Hz), 8.40 (2H, d, $J = 6.6$ Hz). HRMS (EI) m/z calcd for $C_{18}H_{14}N_4O_2$ (M^+) 318.1117, found 318.1110.

5.18. N^1, N^4 -Di(1,3,4-thiadiazol-2-yl)terephthalamide (5b)

Compound **5b** was prepared from 1,3,4-thiadiazol-2-amine, pyridine, and terephthaloyl dichloride using a procedure similar to that described for the preparation of **2** as a white solid. Yield: 31%; mp >300 °C; 1H NMR (300 Hz, DMSO- d_6) δ : 8.24 (4H, s), 9.23 (2H, s). HRMS (EI) m/z calcd for $C_{12}H_8N_6O_2S_2$ (M^+) 332.0150, found 332.0068.

5.19. N^1, N^4 -(4-methylthiazol-2-yl)terephthalamide (5c)

Compound **5c** was prepared from 4-methylthiazol-2-amine, pyridine, and terephthaloyl dichloride using a procedure similar to that described for the preparation of **2** as a white solid. Yield: 12%; mp >300 °C; 1H NMR (300 Hz, DMSO- d_6) δ : 2.30 (6H, s), 6.78 (2H, s), 8.17 (4H, s). HRMS (EI) m/z calcd for $C_{16}H_{14}N_4O_2S_2$ (M^+) 358.0558, found 358.0567.

5.20. N^1, N^3 -Di(pyridin-2-yl)isophthalamide (5d)

Compound **5d** was prepared from pyridin-2-amine, pyridine, and isophthaloyl dichloride using a procedure similar to that described for the preparation of **2** as a white solid. Yield: 52%; mp 253 °C; 1H NMR (300 Hz, DMSO- d_6) δ : 7.36–7.43 (2H, m), 7.68–7.79 (1H, m), 8.09–8.20 (2H, m), 8.23–8.28 (2H, m), 8.30–8.34 (2H, m), 8.48 (2H, d, $J = 1.8$ Hz), 8.59 (0.5H, s), 8.73 (0.5H, s). HRMS (EI) m/z calcd for $C_{18}H_{14}N_4O_2$ (M^+) 318.1117, found 318.1116.

5.21. N^2, N^6 -Di(pyridin-2-yl)pyridine-2,6-dicarboxamide (5e)

Compound **5e** was prepared from pyridin-2-amine, pyridine, and pyridine-2,6-dicarbonyl dichloride using a procedure similar to that described for the preparation of **2** as a white solid. Yield: 8%; mp 228–229 °C; 1H NMR (300 Hz, DMSO- d_6) δ : 7.25 (2H, t, $J = 9.6$ Hz), 7.93 (2H, t, $J = 5.4$ Hz), 8.31 (3H, t, $J = 6.6$ Hz), 8.40 (2H, d, $J = 5.7$ Hz), 8.49 (2H, dd, $J = 0.9$ Hz, 4.5 Hz). HRMS (EI) m/z calcd for $C_{17}H_{13}N_5O_2$ (M^+) 319.1069, found 319.1069.

5.22. N^1, N^3 -Di(thiazol-2-yl)isophthalamide (5f)

Compound **5f** was prepared from thiazol-2-amine, pyridine, and isophthaloyl dichloride using a procedure similar to that described for the preparation of **2** as a white solid. Yield: 71%; mp 285–287 °C; 1H NMR (300 Hz, DMSO- d_6) δ : 7.27 (1H, d, $J = 3.5$ Hz), 7.29 (1H, d, $J = 3.9$ Hz), 7.55 (1H, d, $J = 3.7$ Hz), 7.56 (1H, d, $J = 3.9$ Hz), 7.65–7.73 (1H, m), 8.26 (2H, d, $J = 1.8$ Hz), 8.27 (1H, d, $J = 1.8$ Hz), 8.62 (0.5H, t, $J = 3.3$ Hz), 8.77 (0.5H, t, $J = 3.8$ Hz). HRMS (EI) m/z calcd for $C_{17}H_{13}N_5O_2$ (M^+) 330.0245, found 330.0233.

5.23. 2-(4-Phenylpiperazin-1-yl)-*N*-(thiazol-2-yl)acetamide (3)

A solution of thiazol-2-amine (200 mg, 2 mmol) and anhydrous potassium carbonate (414 mg, 3 mmol) in THF (20 mL) was added with 2-chloroacetyl chloride (339 mg, 3 mmol) dropwise. Then the mixture was stirred under reflux for 2 h. After evaporation THF, the residue was dissolved with water and the precipitate was collected by filtration. A mixture of the obtained acetamide (232 mg, 1.32 mmol), 1-phenylpiperazine (213 mg, 1.32 mmol), and anhydrous potassium carbonate (273 mg, 1.98 mmol) in THF was reacted under reflux for 4 h using potassium iodide as catalyzer. The reaction mixture was evaporated and water was added

subsequently, and then the pH value was adjusted to neutral using 1 M aqueous hydrochloric acid solution. Compound **3** was collected by filtration, water washing, and purification as a slight yellow solid (352 mg, 88% total yield). Mp 167–168 °C; ¹H NMR (300 Hz, CD₃OD-*d*₄) δ: 2.77 (4H, t, *J* = 9.7 Hz), 3.26 (4H, t, *J* = 9.7 Hz), 3.37 (2H, s), 6.83 (1H, t, *J* = 14.6 Hz), 6.98 (2H, d, *J* = 9.8 Hz), 7.14 (1H, d, *J* = 3.9 Hz), 7.21–7.25 (2H, m), 7.44 (1H, d, *J* = 3.7 Hz). HRMS (EI) *m/z* calcd for C₁₅H₁₈N₄OS (M⁺) 302.1201, found 302.1204.

5.24. 2-(4-(2-Fluorophenyl)piperazin-1-yl)-N-(thiazol-2-yl)acetamide (**6a**)

Compound **6a** was prepared from thiazol-2-amine, 2-chloroacetyl chloride, and 1-(2-fluorophenyl)piperazine using a procedure similar to that described for the preparation of **3** as a white solid. Total yield: 69%; mp 159–160 °C; ¹H NMR (300 Hz, CD₃OD-*d*₄) δ: 2.79 (4H, t, *J* = 9.4 Hz), 3.17 (4H, t, *J* = 10.2 Hz), 3.38 (2H, s), 6.93–7.00 (1H, m), 7.02–7.11 (3H, m), 7.14 (1H, d, *J* = 3.8 Hz), 7.44 (1H, d, *J* = 3.7 Hz). HRMS (EI) *m/z* calcd for C₁₅H₁₇FN₄OS (M⁺) 320.1107, found 320.1097.

5.25. 2-(4-(2-Fluorophenyl)piperazin-1-yl)-N-(3-(trifluoromethyl)phenyl)acetamide (**6b**)

Compound **6b** was prepared from 3-(trifluoromethyl)benzenamine, 2-chloroacetyl chloride, and 1-(2-fluorophenyl)piperazine using a procedure similar to that described for the preparation of **3** as a white solid. Total yield: 75%; mp 93–95 °C; ¹H NMR (300 Hz, DMSO-*d*₆) δ 2.70 (4H, t, *J* = 8.8 Hz), 3.09 (4H, t, *J* = 9.2 Hz), 3.24 (2H, s), 6.95–6.99 (1H, m), 7.05–7.16 (3H, m), 7.41 (1H, d, *J* = 7.7 Hz), 7.56 (1H, t, *J* = 15.6 Hz), 7.90 (1H, d, *J* = 8.3 Hz), 8.16 (1H, s). HRMS (EI) *m/z* calcd for C₁₉H₁₉F₄N₃O (M⁺) 381.1464, found 381.1472.

5.26. 2-(4-(2-Methoxyphenyl)piperazin-1-yl)-N-(3-(trifluoromethyl)phenyl)acetamide (**6c**)

Compound **6c** was prepared from 3-(trifluoromethyl)benzenamine, 2-chloroacetyl chloride, and 1-(2-methoxyphenyl)piperazine using a procedure similar to that described for the preparation of **3** as a white solid. Total yield: 70%; mp 95–100 °C; ¹H NMR (300 Hz, DMSO-*d*₆) δ 2.68 (4H, t, *J* = 8.6 Hz), 2.99–3.04 (4H, t, *J* = 8.6 Hz), 3.23 (2H, s), 3.77 (3H, s), 6.87–6.95 (4H, m), 7.43 (1H, d, *J* = 8.0 Hz), 7.56 (1H, t, *J* = 16.1 Hz), 7.89 (1H, d, *J* = 8.5 Hz), 8.16 (1H, s). HRMS (EI) *m/z* calcd for C₂₀H₂₂F₃N₃O₂ (M⁺) 393.1664, found 393.1669.

Acknowledgments

We gratefully acknowledge generous support from the National Natural Science Foundation of China (Grants 20372069, 29725203, and 20472094), the Basic Research Project for Talent Research Group from the Shanghai Science and Technology Commission, the Key Project from the Shanghai Science and Technology Commission (Grant 02DJ14006), the Key Project for New Drug

Research from CAS, and the 863 Hi-Tech Program of China (Grants 2006AA020402, 2006AA020602).

Supplementary data

The features of pharmacophores derived from the GP–ligand complexes for four different binding sites. This material is available free of charge via the Internet at <http://www.sciencedirect.com>. Supplementary data associated with this article can be found, in the online version, at [doi:10.1016/j.bmc.2007.08.003](https://doi.org/10.1016/j.bmc.2007.08.003).

References and notes

- Gershell, L. *Nat. Rev. Drug Discov.* **2005**, *4*, 367–368.
- Tadayyon, M.; Smith, S. A. *Expert Opin. Invest. Drugs* **2003**, *12*, 307–324.
- Guertin, K. R.; Grimsby, J. *Curr. Med. Chem.* **2006**, *13*, 1839–1843.
- Hampson, L. J.; Arden, C.; Agius, L.; Ganotidis, M.; Kosmopoulou, M. N.; Tiraidis, C.; Elemes, Y.; Sakarellos, C.; Leonidas, D. D.; Oikonomakos, N. G. *Bioorg. Med. Chem.* **2006**, *14*, 7835–7845.
- Oikonomakos, N. G.; Skamnaki, V. T.; Tsitsanou, K. E.; Gavalas, N. G.; Johnson, L. N. *Struct. Fold. Design* **2000**, *8*, 575–584.
- Kristiansen, M.; Andersen, B.; Iversen, L. F.; Westergaard, N. J. *Med. Chem.* **2004**, *47*, 3537–3545.
- Oikonomakos, N. G.; Tiraidis, C.; Leonidas, D. D.; Zographos, S. E.; Kristiansen, M.; Jessen, C. U.; Nørskov-Lauritsen, L.; Agius, L. *J. Med. Chem.* **2006**, *49*, 5687–5701.
- Henke, B. R.; Sparks, S. M. *Mini-Rev. Med. Chem.* **2006**, *6*, 845–857.
- Oikonomakos, N. G.; Kosmopoulou, M.; Zographos, S. E.; Leonidas, D. D.; Chrysina, E. D.; Somsak, U.; Nagy, V.; Praly, J. P.; Docsa, T.; Toth, A.; Gergely, P. *Eur. J. Biochem.* **2002**, *269*, 1684–1696.
- Oikonomakos, N. G.; Schnier, J. B.; Zographos, S. E.; Skamnaki, V. T.; Tsitsanou, K. E.; Johnson, L. N. *J. Biol. Chem.* **2000**, *275*, 34566–34573.
- Lu, Z. J.; Bohn, J.; Bergeron, R.; Deng, Q. L.; Ellsworth, K. P.; Geissler, W. M.; Harris, G.; McCann, P. E.; McKeever, B.; Myers, R. W.; Saperstein, R.; Willoughby, C. A.; Yao, J.; Chapman, K. *Bioorg. Med. Chem. Lett.* **2003**, *13*, 4125–4128.
- Wright, S. W.; Rath, V. L.; Genereux, P. E.; Hageman, D. L.; Levy, C. B.; McClure, L. D.; McCoid, S. C.; McPherson, R. K.; Schelhorn, T. M.; Wilder, D. E.; Zavadski, W. J.; Gibbs, E. M.; Treadway, J. L. *Bioorg. Med. Chem. Lett.* **2005**, *15*, 459–465.
- Whittamore, P. R. O.; Addie, M. S.; Bennett, S. N. L.; Birch, A. M.; Butters, M.; Godfrey, L.; Kenny, P. W.; Morley, A. D.; Murray, P. M.; Oikonomakos, N. G.; Otterbein, L. R.; Pannifer, A. D.; Parker, J. S.; Readman, K.; Siedlecki, P. S.; Schofield, P.; Stocker, A.; Taylor, M. J.; Townsend, L. A.; Whalley, D. P.; Whitehouse, J. *Bioorg. Med. Chem. Lett.* **2006**, *16*, 5567–5571.
- Birch, A. M.; Kenny, P. W.; Oikonomakos, N. G.; Otterbein, L.; Schofield, P.; Whittamore, P. R. O.; Whalley, D. P. *Bioorg. Med. Chem. Lett.* **2007**, *17*, 394–399.
- Martin, W. H.; Hoover, D. J.; Armento, S. J.; Stock, I. A.; McPherson, R. K.; Danley, D. E.; Stevenson, R. W.; Barrett, E. J.; Treadway, J. L. *Proc. Natl. Acad. Sci. U.S.A.* **1998**, *95*, 1776–1781.

16. Wolber, G.; Langer, T. *J. Chem. Inf. Model* **2005**, *45*, 160–169.
17. Oikonomakos, N. G.; Schnier, J. B.; Zographos, S. E.; Skamnaki, V. T.; Tsitsanou, K. E.; Johnson, L. N. *J. Biol. Chem.* **2000**, *275*, 34566–34573.
18. Oikonomakos, N. G.; Kosmopoulou, M.; Zographos, S. E.; Leonidas, D. D.; Chrysina, E. D.; Somsak, L.; Nagy, V.; Praly, J. P.; Docsa, T.; Toth, B.; Gergely, P. *Eur. J. Biochem.* **2002**, *269*, 1684–1696.
19. Oikonomakos, N. G.; Tsitsanou, K. E.; Zographos, S. E.; Skamnaki, V. T.; Goldmann, S.; Bischoff, H. *Protein Sci.* **1999**, *8*, 1930–1945.
20. Klabunde, T.; Wendt, K. U.; Kadereit, D.; Brachvogel, V.; Burger, H. J.; Herling, A. W.; Oikonomakos, N. G.; Kosmopoulou, M. N.; Schmoll, D.; Sarubbi, E.; von Roedern, E.; Schonafinger, K.; Defossa, E. *J. Med. Chem.* **2005**, *48*, 6178–6193.
21. Kristiansen, M.; Andersen, B.; Iversen, L. F.; Westergaard, N. *J. Med. Chem.* **2004**, *47*, 3537–3545.
22. Whittamore, P. R.; Addie, M. S.; Bennett, S. N.; Birch, A. M.; Butters, M.; Godfrey, L.; Kenny, P. W.; Morley, A. D.; Murray, P. M.; Oikonomakos, N. G.; Otterbein, L. R.; Pannifer, A. D.; Parker, J. S.; Readman, K.; Siedlecki, P. S.; Schofield, P.; Stocker, A.; Taylor, M. J.; Townsend, L. A.; Whalley, D. P.; Whitehouse, J. *Bioorg. Med. Chem. Lett.* **2006**, *16*, 5567–5571.
23. Oikonomakos, N. G.; Zographos, S. E.; Skamnaki, V. T.; Archontis, G. *Bioorg. Med. Chem.* **2002**, *10*, 1313–1319.
24. Birch, A. M.; Kenny, P. W.; Oikonomakos, N. G.; Otterbein, L.; Schofield, P.; Whittamore, P. R.; Whalley, D. P. *Bioorg. Med. Chem. Lett.* **2007**, *17*, 394–399.
25. 4.10, C. Accelrys, Inc.; San Diego, CA; 2005.
26. Morris, G. M.; Goodsell, D. S.; Halliday, R. S.; Huey, R.; Hart, W. E.; Belew, R. K.; Olson, a. J. *J. Comp. Chem.* **1998**, *19*, 1639–1662.
27. Cornell, W. D.; Cieplak, P.; Bayly, C. I.; Gould, I. R.; Merz, K. M.; Ferguson, D. M.; Spellmeyer, D. C.; Fox, T.; Caldwell, J. W.; Kollman, P. A. *J. Am. Chem. Soc.* **1995**, *117*, 5179–5197.
28. Deng, Q.; Lu, Z.; Bohn, J.; Ellsworth, K. P.; Myers, R. W.; Geissler, W. M.; Harris, G.; Willoughby, C. A.; Chapman, K.; McKeever, B.; Mosley, R. *J. Mol. Graph Model* **2005**, *23*, 457–464.
29. Cleves, A. E.; Jain, A. N. *J. Med. Chem.* **2006**, *49*, 2921–2938.
30. Li, H.; Gao, Z.; Kang, L.; Zhang, H.; Yang, K.; Yu, K.; Luo, X.; Zhu, W.; Chen, K.; Shen, J.; Wang, X.; Jiang, H. *Nucleic Acids Res.* **2006**, *34*, W219–W224 (Web Server issue).
31. Wallace, A. C.; Laskowski, R. A.; Thornton, J. M. *Protein Eng.* **1995**, *8*, 127–134.